

# **Towards Pedestrian Microclimatic Comfort: A Rapid Predication Model for Street Winds and Pedestrian Thermal Sensation**

Jing Li

*Department of Architecture, North China University of Technology  
No. 5, Jinyuanzhuang Road, Shijingshan District,  
Beijing, P. R. China*

Mengnan Qi

*China Construction Engineering Design Group Corporation Limited  
No. 15, Sanlihe Road, Haidian District, Beijing, P. R. China*

Qihua Duan

*Department of Civil and Architectural Engineering  
and Construction Management, University of Cincinnati  
Cincinnati, OH 45221, US*

Lei Huo

*Department of Mathematics and Statistics  
Missouri University of Science and Technology  
Rolla, MO 65409, US*

Julian Wang

*School of Architecture and Interior Design  
Department of Civil and Architectural Engineering  
and Construction Management, University of Cincinnati  
Cincinnati, OH 45221, US  
[Julian.wang@uc.edu](mailto:Julian.wang@uc.edu)*

Accepted 15 May 2018

Published 18 June 2018

Significant changes in the urban built environment have occurred due to rapid urbanization and increases in the urban population. Such alterations may produce environmental health-related issues such as urban heat stress, air pollution and traffic noise. This research undertook a field study to collect data including urban design parameters, micro-environmental factors and city climatic information. This work was conducted over a two-year period on three pedestrian streets located in high-density urban areas in Beijing. These areas were selected in order to study the influences of urban street canyon texture within a particular geometric layout, wind flow corridors and variations in air temperature on pedestrian microclimatic comfort. The results will facilitate the work of urban planners by providing them with information for use in improving outdoor thermal comfort through their designs. A total of 60 485 samples were organized into

training, validation and test sets. We confirmed our hypothesis that internal wind speed ( $W_i$ ) is attributable mainly to the urban texture coefficient ( $U_0$ ), air temperature ( $T$ ) and leading-in wind speed ( $W_{\cos}$ ). The model was tested using the test data collected onsite, which demonstrated a very accurate goodness-of-fit; the model achieved an  $R$ -squared value of 0.82, which meant that  $W_i$  as a dependent variable was 82% correlated to the three predictors as independent variables. With this computer simulation, urban planners can now predict and visualize the impact of changes on the built environment in terms of either the direction of solar radiation received or increases in wind speed, in return for the desired thermal comfort level for residents of the neighborhood.

**Keywords:** Thermal sensation; built environment; urban microclimate; healthcare urban design.

## 1. Introduction

The World Health Organization believes that the warming and precipitation trends attributable to anthropogenic climate change that have become prominent in the last 30 years already claim over 150 000 lives annually. Many human diseases ranging from cardiovascular mortality to respiratory illnesses and the transmission of infectious diseases have been linked to climate fluctuations and heat waves. However, uncertainty remains regarding the attribution to climate change of disease expansion and resurgence, since there is a lack of long-term, high-quality datasets and the well-recorded influence of socio-economic factors and changes in immunity and drug resistance. Patz *et al.* reported on the growing evidence of a climate–health relationship, with future projections of global warming and its impact on climate change possibly increasing the morbidity and mortality rates in many regions around the world.<sup>1</sup>

In 2003, a summer heat wave in Europe killed tens of thousands of people, wilted crops, set forests ablaze, and melted 10% of the Alpine glacial mass. That summer’s blistering heat wave was unprecedented with regards to intensity, duration and geographic extent. More than 200 US cities registered new record high temperatures. Phoenix, Arizona sustained temperatures above 100°F (38°C) for 39 consecutive days, including a week above 110°F (43°C), which took a harsh toll on the homeless. There was also Hurricane Katrina, which gathered steam from the heated Gulf of Mexico and caused devastation in numerous coastal communities.<sup>2</sup>

Potentially vulnerable regions include the temperate latitudes, which are projected to warm disproportionately in regions around the Pacific and

Indian oceans. These areas are currently subjected to significant rainfall variability due to the El Niño/Southern Oscillation phenomenon of sub-Saharan Africa. Sprawling cities where the urban heat island effect could intensify extreme climatic events are also particularly at risk.

In cities, where temperatures tend to be higher than in suburban and rural areas, this generates a phenomenon called Urban Heat Islands (UHIs). This effect occurs primarily because the ever-growing number of buildings has supplanted vegetation and trees. The main causes of these different microclimatic conditions in cities are, among others, urban geometry, which influences incoming and outgoing radiation, and surface material properties such as color and texture. In hot climates, the elevated surface temperatures of materials directly affect not only the urban microclimate, but also the thermal comfort conditions in urban open spaces.

China has witnessed a massive migration across the country from suburban and rural areas to towns and cities by citizens searching for employment; this has led to rapid urbanization in many metropolitan areas, especially in the most prosperous parts of China such as Beijing, Shanghai and Guangzhou. The demand for resources to sustain the basic needs of these inhabitants (such as accommodations, transportation systems to move them between home and work, schools for their children, hospitals for the sick, water, services and resources to support their wellbeing) have all drastically transformed the urban microclimatic conditions.

Studies have confirmed that the characteristics of urban structures play an important part in determining the temperature of a neighborhood.<sup>3–7</sup> For example, it was found in one study that the geometric layout of building architecture, urban landscape and other open spaces could affect the

distribution of airflow and ventilation in surrounding areas, influencing the climatic conditions of the entire neighborhood.<sup>8–10</sup> In other words, the density of urban canyons and urban textures contribute to the microclimatic conditions and determine to a great extent the forms of airflow, solar radiation and ambient temperature. These three major environmental factors significantly influence pedestrian comfort.<sup>1,11–13</sup>

In spite of the existing literature, urban planners and designers are still handicapped by the details they require and limited changes are possible in existing systems. The tools to support and simulate in real-time responses to changes in wind conditions and thermal comfort allow planners to arrive at acceptable outcomes and determine optimal healthcare plans and designs. In conventional urban planning and design practices, either complicated computational analyses by Computational Fluid Dynamics (CFD) or overly simplified strategies with little quantitative information are used to predict, assess and analyze urban microclimatic environment and comfort levels. A new prediction model that can rapidly estimate the urban pedestrian height-level microclimatic conditions and thermal comfort with an acceptable level of resolution is desperately needed.

To address this issue, we conducted a field study of three pedestrian streets in Beijing, China over a two-year period. Our goal was to investigate the relationships among the density of urban canyons, urban textures and microclimatic conditions under the influence of airflow, solar radiation and ambient

temperatures. The data we collected were integrated with historical weather data from the local weather station and urban design parameters extracted from the Geographic Image System (GIS) to develop a model for predicting pedestrian wind conditions and associated thermal sensations in response to different built environment parameters and weather conditions.

## 2. Description of Field Measurements







From studies of urban canyon streets in Beijing, it was found that there were totally 50 municipal special commercial pedestrian streets that had recently been constructed and renovated. The standard layout of the streets is a parallel arrangement throughout the Dongcheng and Xicheng districts. As regards the thermal environment, it has been reported that the level of heat stress is very high, a condition that is made worse by the slow wind flow in dense urban areas.<sup>14</sup> Among these streets, we selected three for our case study: Wangfujing, Qianmen and Dashilan. As shown in Table 1, these three streets are built with narrow canyon spaces, accommodate a high-density population, and experience heavy pedestrian flow.

We undertook field measurements at these three streets to collect microclimatic environment data such as the level of solar radiation, air temperature and wind speed at the pedestrian height-level (1.5 m). The instruments used were an AN100 Anemometer, Extech 42280 Temperature and Humidity Datalogger, and MP-200 Pyranometer Meter.

Table 1. Basic information and spatial features for the three streets.

	Wangfujing street	Qianmen street	Dashilan street
Orientation	North-south (810 m)	North-south (845 m)	East-west (275 m)
Canyon spatial features	Moderate (17 m)	Spacious (20–27.8 m)	Narrow (9–16 m)
Architectural features	A mixture of modern and traditional architecture	Traditional architecture	Traditional architecture
Building height and volume	Mainly high-rise buildings of large size and abundant skyline	2–3 stories and slightly larger sized buildings without obvious height changes	2–3 stories and mainly smaller sized buildings but a larger building size in some areas
Architecture color	Mainly warm colors including brownish red, warm red and warm yellow	Unified, mainly brick gray	White, gray, reddish brown and dark green
Ground pavement	Square brick, undressed granite and smooth granite	Local stone, bluestone, white stone	Bluestone
Landscape greening	Ginkgo trees with small crowns	Sophora japonica with large crowns and dense leaves	Almost no green spaces
Activity level	High	Moderate	Moderate

Table 1. (Continued)

	Wangfujing street	Qianmen street	Dashilan street
Façade view of each street	 <p>Section of eastern facade along Wangfujing Street</p>  <p>Other section of eastern facade along Wangfujing Street</p>  <p>Section of eastern facade along Qianmen Street</p>  <p>Other section of eastern facade along Qianmen Street</p>  <p>Section of northern facade along Dashilan Street</p>  <p>Section of southern facade along Dashilan Street</p>		

Data were collected daily between 10:00AM and 8:00PM from July 1st to August 31st of 2015, and between 10:00AM and 5:00PM from January 1st and February 29th of 2016. The data sampling rate was recordings every 15–20 min. All of the selected data collection spots are shown in Figs. 1–3.

In total, 60 485 data points were collected from these three streets. At the same time, we also studied the urban design elements such as the forms of public spaces, landscape structures, green components and building façade geometry, as well as all other factors that might contribute to pedestrian thermal sensations. Figures 4–6 summarize the daily

average temperatures, horizontal solar radiation and wind speed values collected at these three selected streets during the field study.

Because of the differences in spatial form among these three pedestrian streets, there were also variations in their microclimatic environments. The effects of wind speed attenuation in summer were similar among all three; the smallest attenuation space was in District B of Qianmen Street, and the largest was in District A of Qianmen Street. The same street had completely different wind environments. The main reason for this was that the building density and volume ratio in the two areas

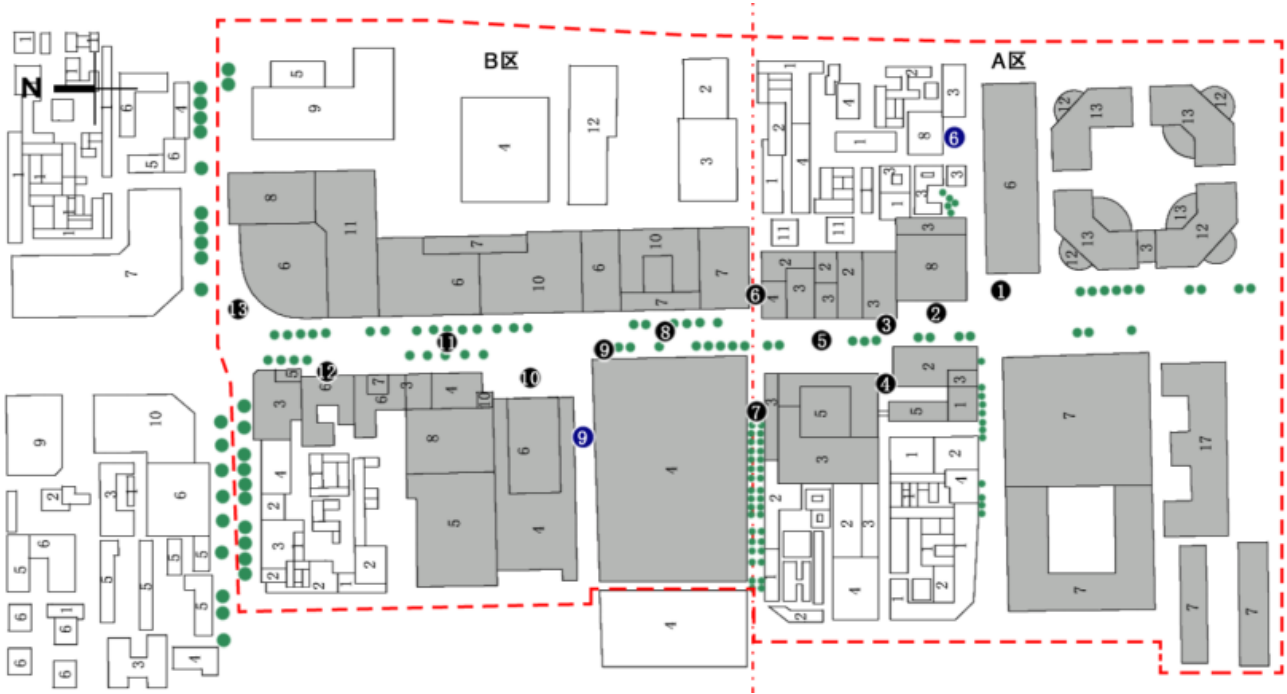


Fig. 1. Area of sampling points at Wangfujing Street.



Fig. 2. Area of sampling points at Qianmen Street.

were significantly different. Spaces with smaller building densities and volume ratios had a hindering effect on wind speed that was relatively small. The area with the greatest influence on wind speed attenuation was District B of Wangfujing Street, followed by the Dashilan commercial street. Both showed that the attenuation of the buildings on the prevailing wind in summer was higher in the vertical space.

This had a hindering effect on part of the airflow, resulting in an attenuation of the wind speed. The wind environment in District A of Qianmen Street was relatively bad, which meant that the unified heights of the buildings or similar areas were more harmful to the windbreak. In our preliminary analysis, we found that based on the data actually measured and the results outlined above, the main factors influencing differences in the wind





Fig. 3. Area of sampling points at Dashilan Street.

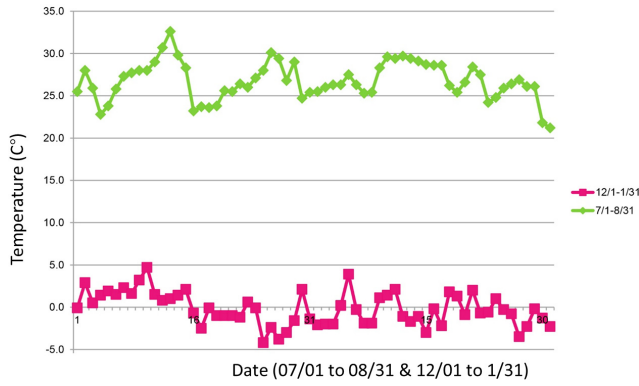


Fig. 4. Daily average temperature recorded at the three streets.

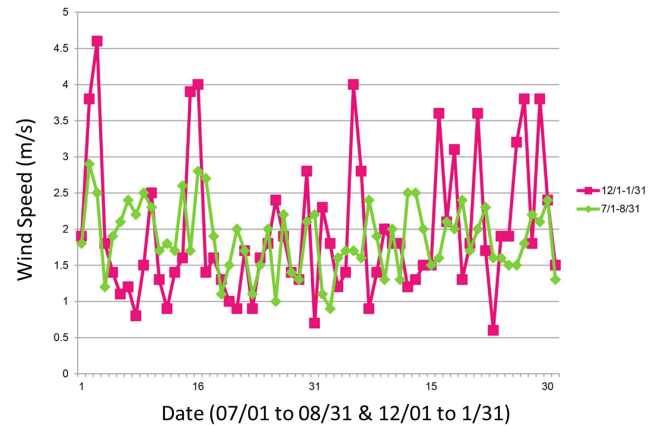


Fig. 6. Daily average wind speed recorded at the three streets.

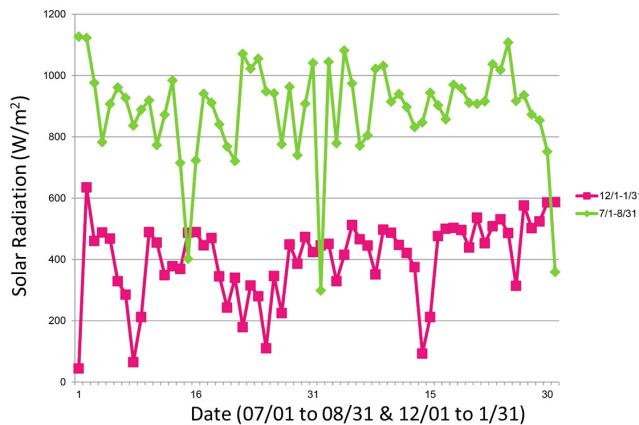


Fig. 5. Daily average solar radiation recorded at the three streets.

environments of pedestrian streets include building density, volume ratio, street direction, street width, building layout, differences in building height, building volume, continuity of building interfaces, buildings' corner shapes and forms, glass roofs, overhangs on ground floors, corridors, open space forms, landscape elements and other structures.

### 3. Development of the Pedestrian Comfort Model

#### 3.1. Existing wind estimation models

In order to provide an effective and accurate model for urban planners and architects to visualize the wind flow patterns and air distribution within an

urban built environment, researchers over the years have developed a number of systems based on CFD<sup>14</sup> to calculate pedestrian wind conditions. These are organized according to the following resolutions:

- Regions (within 100–200 km),
- Cities (within 10–20 km),
- Neighborhoods (within 1–2 km), and
- Streets (within 100–200 m).

These include the Mellor-Yamada hierarchical model,<sup>15,16</sup> NCAR rapid prediction models<sup>17</sup> and Kubota's climate study and prediction model<sup>18,19</sup> for the computation of average wind speeds at the required points on a block.<sup>20,21</sup> However, most of these systems are unable to respond to real-time changes in terms of temperature, solar radiation or wind speed within their scales, and are concerned only with predicting the thermal sensation outcomes accordingly.

In 2014, Ng *et al.*<sup>22</sup> proposed a semi-empirical morphological model that integrates the geometrical parameters of the associated cities and buildings concerned, including the façade area density,  $\lambda_f$ , and coverage density,  $\lambda_p$ , with the geometric or morphological parameters associated with the urban buildings obtained from urban GIS models.<sup>23,24</sup> Furthermore, these systems also integrated wind environmental data under experimental conditions, including rough degrees of facade and airflow displacement height, etc., into the system, and showed a strong correlation to the wind environment on the pedestrian scale of urban streets.<sup>25</sup> Bentham and Britter further enhanced the idea of predicting wind speeds on streets at different heights in a vertical direction.<sup>26</sup> This traditional, semi-empirical model form can quickly be applied in order to achieve support for planning and design decisions in the initial design phase of land use and urban density analyses.

However, the application of these semi-empirical models generally limits the facade's area density,  $\lambda_f$ , to between 0.01 and 0.3; the facade area density involved in pedestrian height measurement points on high-density urban blocks is usually higher than 0.3.<sup>22,27,28</sup> Bentham and Britter's analysis also found that the accuracy of the model is greatly reduced when the façade area density,  $\lambda_f$ , is more than 0.3, when the interaction of high-density buildings and wind speed variables in the street does not conform to the logarithmic relationship defined

by the original model.<sup>29</sup> Furthermore, this semi-empirical model is based on wind environment analyses in large-scale spatial forms, focusing on the spatial distribution and patterns of motion in the wind corridor, including wind direction, wind tension and trend. For street and neighborhood lengths ranging from a few hundred meters to one kilometer, the average wind speed variable becomes more important in determining the thermal comfort and air quality of the outdoor environment.<sup>30</sup> Here, we propose a new predictive model for pedestrian wind conditions using urban canyons' morphological parameters and external weather features as independent variables.

### 3.2. Fine-scale wind estimation model

First, we introduced three parameters to help study wind estimation models and predict wind speed at pedestrian height-level. These parameters were:

- the point-related façade area density,  $\lambda_{f\text{-point}}$ , which is the ratio between the façade area of all buildings at the target point position, its height, and the overall site area within the  $L$ -radius circle;
- $\lambda_{p\text{-point}}$ , which is the ratio between the built area at the target point position, its height, and the overall site area within the  $L$ -radius circle; and
- a distance index ( $L$ ) from individual buildings to the target point.

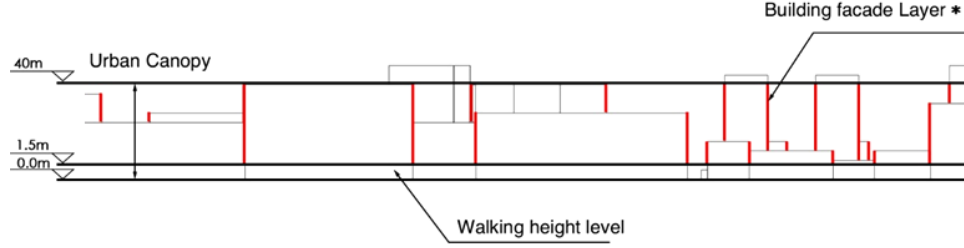
Two schematic illustrations of  $\lambda_{f\text{-point}}$  and  $\lambda_{p\text{-point}}$  are shown in Figs. 7 and 8. The estimations of the wind speeds are referenced from the target points rather than the overall street canyon and can be further refined to generate wind speed distributions in real-time for urban planners seeking to visualize this in the early design stage.

Second, the current research showed that the wind speed at a certain height correlates strongly with  $\lambda_{f\text{-point}}$  and  $\lambda_{p\text{-point}}$ . Therefore, we integrated these urban morphological parameters into the model to capture the important independent variables. We propose an urban texture coefficient,  $U_0$ , which is defined in Eq. (1) as follows:

$$U_0 = \left( \frac{2(1 - \lambda_{p\text{-point}})}{\lambda_{f\text{-point}}} \right)^{0.5}, \quad (1)$$

where:

- $\lambda_{f\text{-point}}$  is the ratio of the overall building facade area to the area of the  $L$ -radius covering the site

Fig. 7. Schematic illustration of the  $\lambda_{f\text{-point}}$  calculation approach.Fig. 8. Schematic illustration of the  $\lambda_{p\text{-point}}$  calculation approach.

- at the target point above 1.5 m; and
- $\lambda_{p\text{-point}}$  is the ratio of the building area to the area of the  $L$ -radius covering the site at the target point position at the target point above 1.5 m.

Third, based on the field measurement data collected, we undertook a correlation analysis of wind

speed values ( $W_i$ ) at the collected points and the external climatic parameters, including the following variables listed in Table 2, below.

Among these variables, the leading-in wind speed was calculated based on the imported wind angles — relative direction in this study — which is defined as the angle between the external wind direction and the street orientation angle. The schematic illustration is shown in Fig. 9, above.

Figure 10 shows the pairwise relationships among these variables, in which both  $U_0$  and  $W_{\cos}$  have approximate linear relationships with the internal wind speed,  $W_i$ . Wind speed,  $W_i$ , has different ranges and levels and behaves differently according to the temperature,  $T$ . The other variables were not strongly inter-correlated.

Fourth, we undertook several regression models using  $W_i$  as a dependent variable, in response to the three independent variables defined by Eq. (2) during the training cycle:

$$W_i = f(U_0, W_{\cos}, T). \quad (2)$$

The learning was in stepwise iterations and designed to search for optimization using a selected set of values for the parameters as inputs to the algorithm.

Finally, the Mean Squared Prediction Error (MSPE), defined in Eq. (3), was used to identify the

Table 2. Parameters analyzed in the correlation study.

External wind relative direction (based on the main direction of the street's central axis)	$W_d$
External wind speed	$W_s$
Wind speed differential	$W_{rw} (W_{rw} = (W_s - W_i)/W_s)$
Leading-in wind speed	$W_{\cos} (W_{\cos} = W_s * \cos(W_d))$
Air temperature	$T$
Urban texture coefficient	$U_0$



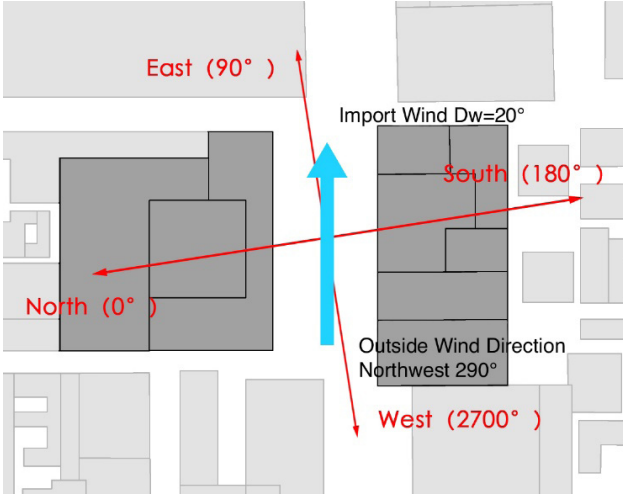


Fig. 9. Schematic illustration of the external wind's relative direction for leading-in wind calculations.

best set of results with maximum accuracy.

$$\text{MSPE} = \text{ave}\{(\text{predicted } W_i - \text{actual } W_i)^2\}. \quad (3)$$

To ensure the validity and reliability of the model we developed, we divided the 60 485 samples into three populations, without duplication. These included training, validation and test sets. In the process, 50% of the population (30 242 samples) was selected as the training set to fit the model; the other 50% was further split into 25% (15 121 samples) each, for the respective purposes of validation and testing. The training used the MSPE to identify the optimized multivariable tuples as concepts for use in prediction:

$$W_i = U_0 e^{(4.7 - 0.9W_{\cos} - 0.24T + 0.1W_{\cos} * T)}. \quad (4)$$

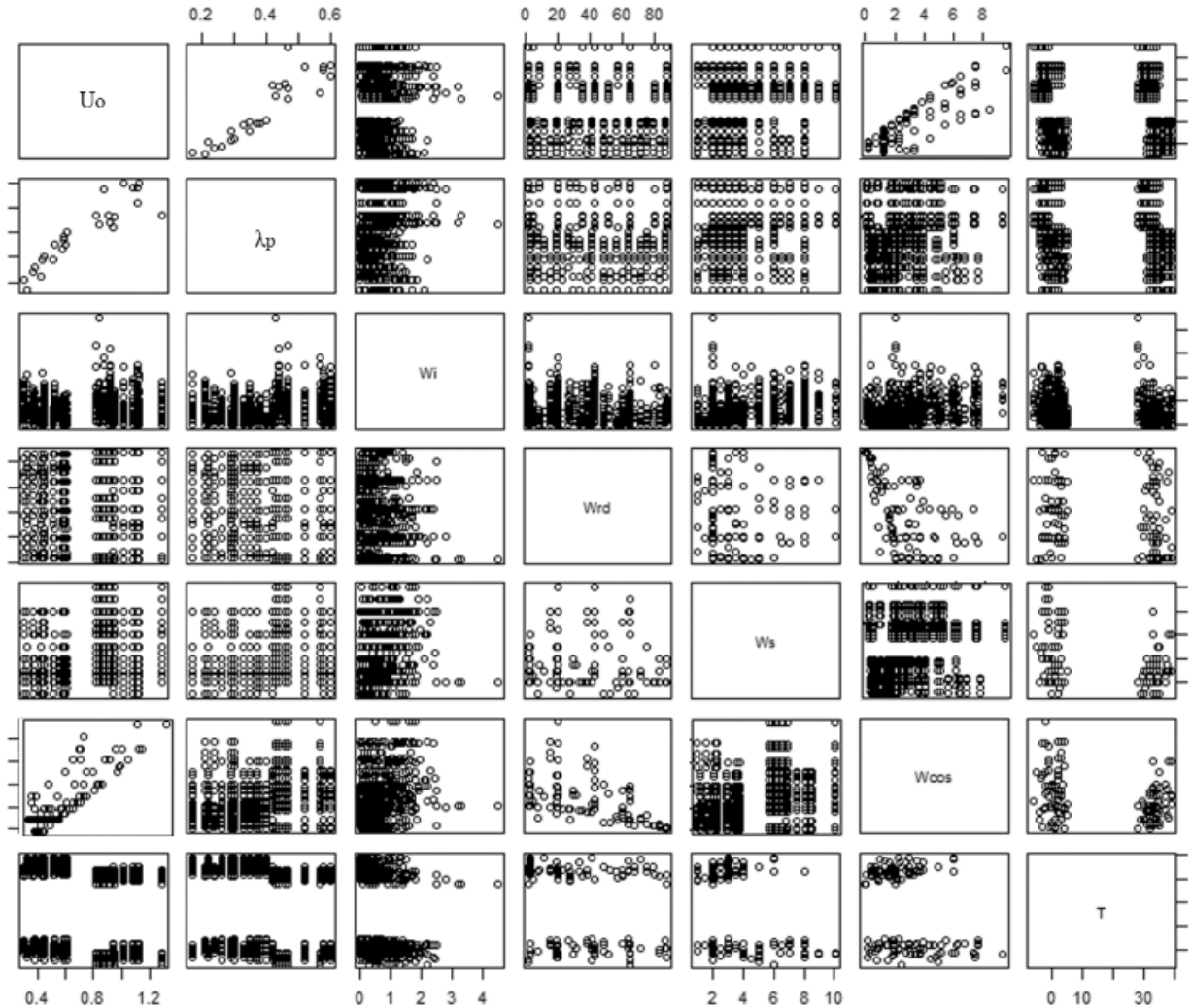


Fig. 10. Pair-wise relationships among the variables.

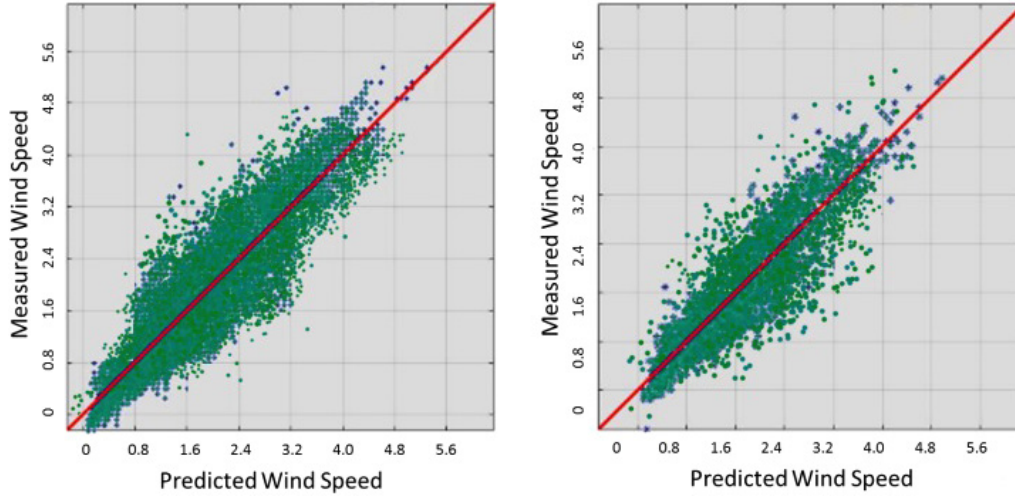


Fig. 11. Fit goodness for the training and testing data.

Using the function shown in Eq. (4), the  $R$ -squared of the above model was 0.82, which meant that 82% of the variability in  $W_i$  could be attributed solely to the following five predictors: the density of urban canyons, their textures, urban airflow, solar radiation and ambient temperature. The model was tested using the test data to obtain the very accurate goodness-of-fit featured in Fig. 10. The MSPE for this model was 0.004, and the data points were, in general, very close to the red line, which is the locus of where there is no error between the predicted and actual values. Moreover, the scatter of data points was almost identical in both plots, confirming that the model did not suffer from problems of under- or over-fitting.

Applying Eq. (1) to Eq. (4) forms the fine-scale wind estimation model of Eq. (5):

$$W_i = \left( \frac{2(1-\lambda_{p\text{-point}})}{\lambda_{f\text{-point}}} \right)^{0.5} * e^{(4.7-0.9W_{\cos}-0.24T+0.1W_{\cos}*T)}. \quad (5)$$

### 3.3. Outdoor thermal comfort modeling

Once the hypothesis that internal wind speed ( $W_i$ ) can be attributed mainly to the urban texture coefficient ( $U_0$ ), air temperature ( $T$ ) and leading-in wind speed ( $W_{\cos}$ ) was confirmed, we proceeded to study the most suitable index as output for urban planners to use in assessing outdoor thermal comfort. In this context, there is a wide spectrum of choices ranging from the Predicted Mean Vote (PMV) to the Physiological Equivalent Temperature

(PET), Universal Thermal Climate Index (UTCI), Thermal Sensation Vote (TSV), Thermal Sensation Index (TSI) and Index of Thermal Stress (ITS).

For instance, Spagnolo *et al.* studied various outdoor locations in Australia and found that there was a wider “comfort zone” as compared to the indoor thermal environment.<sup>31</sup> Berkovic *et al.* evaluated the PMV index in outdoor conditions in a hot and arid climate.<sup>32</sup> PET has also been widely applied and tested in different climatic zones.<sup>33,34</sup> In general, it was found that appropriate outdoor thermal comfort index selection was highly dependent upon the climatic conditions in the regions concerned. Therefore, in this research we decided to adopt the TSI outdoor thermal comfort calculation model, based on research studies undertaken in Japan for both the summer and winter seasons.<sup>35</sup> This model has also been tested and determined to be satisfactory in studies of other Asian cities with hot summers and cold winters.<sup>36,37</sup>

The TSI adopted in our model ranges from 0 (very cold) to 7 (unbearably hot), with 4 as the most comfortable or thermally neutral condition, in which one does not experience any thermal discomfort.<sup>35</sup> The TSI model development process was trained under various solar and wind conditions in order to quantify the experience of outdoor climatic variables in relation to the participants’ subjective feelings of thermal sensation. This model follows the simplified equation [Eq. (5)], taking into account air temperature, solar radiation and wind speed, which can be conveniently integrated into parametrically

driven platforms (e.g., Revit, Rhino, GIS, etc.) and is ready for integration with historical weather data for design and planning practices.

$$\text{TSI} = 1.2 + 0.1115 * T + 0.0019 * R_{dn} - 0.3185 * W_i, \quad (6)$$

where TSI is the TSI ranging from 0 to 7,  $T$  is the air temperature,  $R_{dn}$  is the direct solar radiation and  $W_i$  is the wind speed at the target point.

By combining Eqs. (5) and (6), we were able to obtain the final Thermal Comfort Prediction Model (TCPM) for urban canyons in high-density districts.

$$\text{TSI} = 1.2 + 0.1115 * T + 0.0019 * R_{dn} - 0.3185 * U_0 e^{(4.7 - 0.9W_{\cos} - 0.24T + 0.1W_{\cos} * T)}. \quad (7)$$

#### 4. Application to the Three Streets

Using the TCPM [Eq. (7)] that we developed, one can conveniently calculate the thermal comfort index (TSI) for any position within a street canyon, based only on urban planning/design parameters and historical weather data, and avoiding complex computations and simulations or actual field measurements. To analyze the thermal sensation conditions in these three streets, we randomly selected 60 points along each of the three selected streets in our field study to be input into our prediction model, together with daily average temperature and solar irradiance values. These data were used to compute the estimated thermal comfort indexes in both the summer and winter seasons; the results are presented in Table 3.

The results show that:

- The external thermal environment was apparently outside of the thermal comfort zone for all three streets in both summer and winter, due to the large variations in wind speed; among them, Wangfujing Street showed a larger variance in the

TSI values than the other two streets, due to the geometric variations in the canyon.

- Furthermore, variations in the height of the building along the path also introduce a discrepancy to the computation; compared to the building forms in Wangfujing Street, Qianmen and Dashilan Streets are mainly made up of smaller buildings without obvious changes in height. Therefore, the wind speed values in winter were slightly lower than on Wangfujing Street, resulting in slightly higher TSI values in winter and lower standard deviation values. The findings regarding thermal sensation are consistent with the survey results we found in previous research.<sup>38,39</sup>
- Further analysis of the TSI value distribution of this street revealed that the spatial features indeed contributed to the final TSI values. For instance, the points close to the large-volume buildings and narrow street spaces provided relatively cooler conditions (i.e., the TSI values were lower than average) in summer. However, in the winter scenario, the differences attributable to the street's spatial features were attenuated. This might be due to lower air temperatures and relatively stable wind speeds in winter.

#### 5. Conclusions

Using urban canyons' microclimatic features and the corresponding urban planning and design principles, we developed a TCPM to rapidly estimate pedestrian height-level TSI values. One of the strengths of this method is the time taken to compute the thermal comfort information for urban planners seeking to address specific microclimatic issues related to the thermal environment. For example, if a heat stress concern (e.g., a TSI > 6 at a point) was identified, a new design to adjust the direction of solar radiation received and increase wind speed could be put in place. With the help of this simulator, one can change the corresponding façade area density ( $\lambda_{p\text{-point}}$ ) or site coverage ratio ( $\lambda_{f\text{-point}}$ ) by adjusting building forms and street widths to reduce the heat stress in that zone. Moreover, findings from our previous work illustrate how adjustments made to building and urban design parameters can help to improve environmental variables and user needs.<sup>40,41</sup>

The reliability and validity of the data used for the simulation plays an important role in

Table 3. TSI analysis results.

	Mean		Std. Dev.	
	Summer	Winter	Summer	Winter
Wangfujing street	5.1	1.5	2.4	1.7
Qianmen street	5.3	2.1	1.5	1.3
Dashilan street	5.6	1.3	1.1	1.3

determining the accuracy of the model; for instance, the weather data used in this study are from a local weather station (the Dongcheng District Weather Station), which is geographically closer to the three streets we selected for this field study; this is undoubtedly biased, and unlikely to represent the city as a whole. Therefore, it is important to select local weather stations closer to the streets targeted as reference. Furthermore, the geometric parameters (e.g.,  $\lambda_{p\text{-point}}$  and  $\lambda_{f\text{-point}}$ ) of the predictive model developed in this study were computed on the ArcGIS platform, upon which the smallest allowable separation between two coordinate values in a feature class include  $x$ ,  $y$ ,  $z$  and  $m$  resolution values. Therefore, the resolution of the given map could impact the precision or scale value of the predictive model.

Regarding future work, a more in-depth systematic validation of the proposed model with actual subjective thermal sensation surveys is required to understand the applicability and accuracy of the simulated results and support various urban planning and design purposes. In addition, more functionality should be developed using the Revit API to pave the way for real-time thermal comfort index mapping and visualization, further supporting parametric urban planning for better microclimatic comfort and health.

## Acknowledgments

This project was funded by the National Natural Science Foundation of China (51708002) and the U.S. Environmental Protection Agency (SU-83694001).

## References

1. J. A. Patz, D. Campbell-Lendrum, T. Holloway and J. A. Foley, *Nature* **438**, 310 (2005).
2. P. R. Epstein, *N. Engl. J. Med.* **353**, 1433 (2005).
3. L. Yang and Y. Li, *Energy Build.* **43**, 1139 (2011).
4. M. Kolokotroni, I. Giannitsaris and R. Watkins, *Sol. Energy* **80**, 383 (2006).
5. R. Priyadarsini, W. N. Hien and C. K. Wai David, *Sol. Energy* **82**, 727 (2008).
6. R. A. Memon, D. Y. C. Leung and D. Y. C. Leung, *J. Environ. Sci.* **22**, 1903 (2010).
7. W. Y. Fung, K. S. Lam, W. T. Hung, S. W. Pang and Y. L. Lee, *Energy* **31**, 2287 (2006).
8. V. Shilton, P. Giess, D. Mitchell and C. Williams, *Indoor Built Environ.* **11**, 266 (2002).
9. M. Braniš, J. Hovorka, P. Řezáčová, M. Domasová and M. Lazaridis, *Indoor Built Environ.* **14**, 307 (2005).
10. S. Kato and H. Huang, *J. Wind Eng. Ind. Aerodyn.* **97**, 358 (2009).
11. T. R. Oke, *Boundary Layer Climates* (Routledge, 2002).
12. V. Ok, A. Özsoy, V. Atlı, M. Özgünler and N. Serteser, *TUBITAK (Turkish Sci. Tech. Res. Counc. INTAG-214, İstanbul* (1996).
13. N. Serteser and V. Ok, Urban, The effects of building parameters on wind velocity and air-flow type in the urban settlements, *The 7th International Conference on Urban Climate*, 29 June to 3 July (2009).
14. R. E. Britter and S. R. Hanna, Flow and dispersion in urban areas, *Annu. Rev. Fluid Mech.* **35**, 469 (2003).
15. A. Mochida, et al., *J. Wind Eng. Ind. Aerodyn.* **67**, 459 (1997).
16. S. Murakami, *Int. J. Heat Fluid Flow* **25**, 849 (2004).
17. G. A. Grell, J. Dudhia and D. R. Stauffer, A description of the fifth-generation Penn state/NCAR mesoscale model (MM5). *NCAR Technical Note TN-398+STR 122* (1995).
18. W. C. Skamarock et al., A description of the advanced research WRF Version 2 NCAR Technical Note, *Natl. Cent. Atmos. Res.* **113** (2005).
19. B. Blocken, W. D. Janssen and T. van Hooff, *Environ. Model. Softw.* **30**, 15 (2012).
20. M. O. Letzel, M. Krane and S. Raasch, *Atmos. Environ.* **42**, 8770 (2008).
21. S. Murakami, *Fluid Dyn. Res.* **38**, 108 (2006).
22. C. Yuan and E. Ng, *Urban Clim.* **8**, 57 (2014).
23. T. Kubota, M. Miura, Y. Tominaga and A. Mochida, *Build. Environ.* **43**, 1699 (2008).
24. S. H. L. Yim, J. C. H. Fung, A. K. H. Lau and S. C. Kot, *Atmos. Environ.* **43**, 4982 (2009).
25. C. S. B. Grimmond and T. R. Oke, *J. Appl. Meteorol.* **38**, 1262 (1999).
26. C. Yuan, C. Ren and E. Ng, *Urban Clim.* **10**, 585 (2014).
27. T. Benthams and R. Britter, *Atmos. Environ.* **37**, 2037 (2003).
28. H. Cheng and I. P. Castro, *Boundary-Layer Meteorol.* **104**, 229 (2002).
29. R. W. Macdonald, R. F. Griffiths and D. J. Hall, *Atmos. Environ.* **32**, 1857 (1998).
30. O. Coceal and S. E. Belcher, *Boundary-Layer Meteorol.* **115**, 47 (2005).
31. J. Spagnolo and R. de Dear, *Build. Environ.* **38**, 721 (2003).
32. S. Berkovic, A. Yezioro and A. Bitan, *Sol. Energy* **86**, 1173 (2012).
33. I. Charalampopoulos and I. Tsiros, *Perspectives on Atmospheric Sciences* (Springer, Cham, 2017), pp. 329–334.

34. A. Qaid, H. Bin Lamit, D. R. Ossen and R. N. Raja Shahminan, *Energy Build.* **133**, 577 (2016).
35. B. Givoni *et al.*, *Energy Build.* **35**, 77 (2003).
36. E. Ng and V. Cheng, *Energy Build.* **55**, 51 (2012).
37. N. Gaitani, G. Mihalakakou and M. Santamouris, *Build. Environ.* **42**, 317 (2007).
38. J. Li, M. Qi and T. Chen, *Build. Energy Effic.* **46**, 56 (2017).
39. J. Li, M. Qi and H. Zhang, Field Measurement and Urban Design Analysis on Summer Wind-comfortable Environment in Urban High-density Districts. (2017), pp. 231–236.
40. J. Wang, J. Li and X. Chen, Parametric design based on building information modeling for sustainable buildings, *Int. Conf. Challenges Environ. Sci. Comput. Eng. CESCE 2010* Vol. 2, (2010), pp. 236–239.
41. J. Wang, J. Li, X. Chen and Z. Lv, Developing indoor air quality through healthcare and sustainable parametric method, *Bioinformatics and Biomedical Engineering (iCBBE), 2010 4th International Conference on*, 1–4 (IEEE, 2010).



Copyright of Nano Life is the property of World Scientific Publishing Company and its content may not be copied or emailed to multiple sites or posted to a listserv without the copyright holder's express written permission. However, users may print, download, or email articles for individual use.